Journal of Materials Chemistry B

Accepted Manuscript

ROYAL SOCIETY OF CHEMISTRY

www.rsc.org/materialsB

Journal of Materials Chemistry B

RSCPublishing

ARTICLE

Controlled surface density of RGD ligands for cell adhesion: evidence for a ligand specificity by using QCM-D.

L. Sandrin, D. Thakar, C. Goyer, P. Labbé, D. Boturyn* and L. Coche-Guérente*

Cite this: DOI: 10.1039/x0xx00000x

Received ooth January 2015,
Accepted ooth January 2015

DOI: 10.1039/x0xx00000x

www.rsc.org/

RGD peptides (Arg-Gly-Asp) are known to promote cell adhesion. As a consequence, numerous materials have been functionalized using these peptides for several medical applications. We report herein the controlled functionalization of surface to study the influence of RGD density on cell selectivity. For this purpose, we selected quartz crystal microbalance with dissipation as this technique allows real-time monitoring of cell adhesion to RGD surfaces. We observed that a critical spacing between RGD ligands of nearly 40 nm is required to observe selective cell adhesion whereas higher density is not specific.

Introduction

The controlled and selective cell adhesion to surfaces is essential for a wide range of applications in the field of biomaterials and tissue engineering. For this purpose, extracellular matrix (ECM) and their related synthetic ligands were extensively exploited for tailoring surfaces.[1] ECM components bind to cell receptors such as integrins providing anchoring junctions and the ensuing structural integrity to the cells. The RGD (Arg-Gly-Asp) tripeptide is found in many ECM proteins and was identified as the minimal peptide sequence for cell adhesion through the integrin receptor.[2] To date, RGD peptides were widely used to functionalize surfaces for numerous applications (tissue engineering, implants, tumor cell capture).[3,4] Since this RGD triad is a common integrin binding sequence, our research group and others have focused on the use of a constrained peptide, namely cyclo(-RGDfK-),[5] that specifically homes the $\alpha_V\beta_3$ integrin up-regulated in the tumor microenvironment. The cyclic structure perfectly mimics the physiological RGD loop of the vitronectin which is the natural ligand for the $\alpha_V\beta_3$ integrin. In addition, as multivalency offers enhanced affinity,[6] we designed clustered RGD-containing ligands (Figure 1) with interesting biological properties for cancer applications including imaging-guided surgery[7] and targeted drug delivery.[8] Interestingly, this compound was successfully applied to the selective capture of cells from biological fluids.[9]

Although soluble RGD peptides, including clustered RGD ligands, are highly selective for $\alpha_V\beta_3$-expressing cells, the presentation of immobilized RGD peptides on surface not only determines the cellular behavior[10] but it may also alter the cell selectivity. Non-specific interactions between cells and functional surfaces are mainly governed by positively-charged species on the surface that interact for instance with the negatively charged glycocalyx of cell surface.[11] This last characteristic has often been neglected when RGD peptides are immobilized on a model surface.

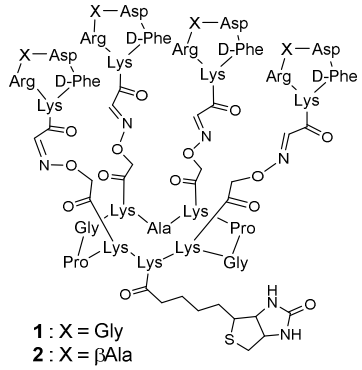

Fig. 1 Peptides (**1** and **2**) structure.

During our continuing work in studying cell adhesion on surface, we designed functionalized-SAMs (self-assembled monolayers) displaying clustered RGD ligands or RβAD as nonsense peptides using biotin-streptavidin bioaffinity interaction (Figure 1). We selected RβAD peptide as it mimics the presence of RGD ligand without its specificity.[9a] In this study, the cell adhesion process was monitored in real-time by combining quartz crystal microbalance with dissipation monitoring (QCM-D) and optical microscopy. QCM-D is an acoustic technique based on the piezoelectric effect providing information on the viscoelastic properties of an adlayer

acoustically bound to the sensor crystal. Changes in resonant frequency (Δf is related to the total oscillating mass) and in energy dissipation of the shear oscillation (ΔD is related to the damping of the acoustic wave)[12] are simultaneously measured. QCM-D is particularly attractive to the field of cell biology as this technique has the potential of monitoring cell-surface interactions in a dynamic and non-invasive way.[13-16] QCM-D technique reflects in real-time, changes in cell-substrate interactions *via* its sensitivity in viscoelasticity and mechanical properties. It has been used to probe changes in attached cells morphology as a function of the nature of the biomaterial sensor surface or in response to external stimuli after cell seeding onto the resonator surface.[17-19] QCM sensors have been also used to monitor specific integrin mediated adhesion of mammalian cells to various adhesive extracellular matrix proteins (fibronectin, vitronectin or laminin) immobilized on the resonator surface.[20-24] But only few papers describing the analysis of cell adhesion process onto functionalized sensor surfaces with cell-adhesive short peptide fragments have appeared in literature.[9b,25,26] To the best of our knowledge few experiments were reported investigating the specificity of RGD functionalized surface in comparison with a variant of RGD such as the RβAD peptide.[9a]

Experimental

Materials.

PBS (Phosphate Buffer Saline), DMEM (Dulbecco's Modified Eagle's Medium), foetal calf serum, penicillin and streptomycin for cell culture were obtained from Gibco. The biotinylated alkanethiol EG_6Biot (2-(2-(2-(2-(2-(2-(1-mercaptoundec-11-yloxy) ethoxy) ethoxy) ethoxy) ethoxy) ethoxy) ethyl biotinamide) was obtained from Prochimia and the hydroxylated alkanethiol EG_4OH ((1-mercaptoundec-11-yl)tetra(ethylene glycol)) was obtained from Aldrich. Ultrapure water was obtained from a Milli-Q Purelab UHQ (Elga) with a resistivity of 18.2 MΩ/cm. Streptavidin from *streptomyces avidinii* was obtained from Sigma. All reactants were analytical grade. Ferrocene methanol, Na_2HPO_4, NaH_2PO_4, KPF_6 and KCl were obtained from Acros organics, NaCl from Fluka, NaOH from Laurylab. The PBS buffer used in QCM experiments consisted of Na_2HPO_4 0.01 M ; NaCl 0.137 M ; KCl 0.0027 M ; pH = 7.4.

General Procedure for Solid-Phase Peptide Synthesis.

Assembly of all protected peptides was carried out using Fmoc/*t*Bu strategy manually in a glass reaction vessel fitted with a sintered glass frit. Coupling reactions were performed using, relative to the resin loading, 1.5-2 equiv of Fmoc-protected amino acid activated in situ with 1.5-2 equiv of PyBOP and 3-4 equiv of DIEA in DMF (10 mL/g resin) for 30 min. Manual syntheses were controlled by Kaiser and/or TNBS tests. Fmoc protecting groups were removed by treatment with a piperidine/DMF solution (1:5) (10 mL/g resin) for 10 min. The process was repeated 3 times, and the completeness of deprotection was verified by the UV absorption of the piperidine washings at 299 nm. Synthetic linear peptides were recovered directly upon acid cleavage (1% TFA in CH_2Cl_2). The resins were treated for 3 min repeatedly until the resin beads became dark purple. The combined washings were concentrated under reduced pressure, and white solid peptides were obtained by precipitation from ether. They were analyzed by RP-HPLC and, if necessary, purified on a preparative column.

General Procedure for Cyclization Reactions.

All linear peptides (0.5 mM) were dissolved in DMF, and the pH was adjusted to 8-9 by addition of DIEA. PyBOP (1.2 equiv) was added, and the solution was stirred at room temperature for 1 h. Solvent was removed under reduced pressure, and the residue dissolved in the minimum of CH_2Cl_2. Ether was added to precipitate the peptide. Then it was triturated and washed 3 times with ether to yield crude material without further purification.

cyclo[-Lys(Boc)-Lys(Alloc)-Lys(Boc)-Pro-Gly-Lys(Boc)-Ala-Lys(Boc)-Pro-Gly-] 3.

The linear peptide H-Lys(Boc)-Lys(Alloc)-Lys(Boc)-Pro-Gly-Lys(Boc)-Ala-Lys(Boc)-Pro-Gly-OH was assembled on Sasrin resin (500 mg) affording 467 mg (0.3 mmol) of a white solid powder. The cyclization reaction was carried out using linear peptide (467 mg, 0.3 mmol) as described above.

cyclo[-Lys-Lys(Biotin)-Lys-Pro-Gly-Lys-Ala-Lys-Pro-Gly-] 4. (see Scheme 1)

Alloc group was removed using cyclic peptide **3** (100 mg, 63 µmol) dissolved in 5.3 mL of dry DCM under argon by adding phenylsilane (330 µl, 2.7 mmol) for 3 min and then $Pd(PPh_3)_4$ (12.4 mg, 10 µmol) for 1 h at room temperature. The solvent was removed under reduced pressure. The crude product **4** was dissolved in the minimum of a solution containing a mixture of CH_2Cl_2 and CH_3OH (1:1). Ether was added to precipitate the crude product. Then it was triturated and washed 3 times with ether. The product **4** is obtained as a white powder. Biotin (15 mg, 60 µmol), PyBOP (33 mg, 60 µmol), and DIEA were then added to a solution containing the cyclic peptide **4** (96 mg, 60 µmol) in 6 mL of DMF to adjust the pH to 8.0. The reaction was stirred for 1 h at room temperature and then concentrated under reduced pressure. The crude product was triturated and washed with ether to yield compound **5** as a white powder. Removal of Boc moieties was carried out in a solution containing 50% TFA in DCM for 1 h at room temperature. The crude product was concentrated, triturated, and washed with ether to yield compound **6** as a white powder (102 mg, 60 µmol, quantitative yield).

Cyclopeptide 7.

($Boc)_2NO-CH_2$-CO-NHS (60 mg, 150 µmol) and DIEA were added to a solution of compound **6** (50 mg, 37 µmol) in 8 mL of DMF to adjust the pH at 8.0. The reaction was stirred for 30 min at room temperature and then concentrated under reduced pressure. The crude product was triturated and washed with ether to yield the expected compound as a white powder. Mass spectrum (ES-MS, positive mode) calcd 2338.2, found 2377.3 $[M + K]^+$. Removal of Boc moieties was carried out in a solution containing 50% TFA/5% TIS/5% H_2O in DCM for 1 h at room temperature. The crude product was concentrated and then purified by RP-HPLC to afford compound **7** as a white powder (12 mg, 7.8 µmol, 21% in two steps). Mass spectrum (ES-MS, positive mode) calcd 1537.8, found 1538.9.

Peptide Derivatives 8 and 9.

The compounds **8** and **9** were prepared as described in the literature by a combination of SPPS and solution strategy.[27]

Peptide Conjugate 1.

To a solution containing the derivative **7** (15 mg, 9.1 µmol) in 1 mL of H_2O/acetonitrile (1:1) was added the peptide **8** (26.3 mg, 40 µmol). The reaction mixture was stirred for 5 h at 25 °C. Conjugate **1** was isolated after purification by RP-HPLC as a white powder (25 mg, 6.1 µmol, 60%). Mass spectrum (ES-MS, positive mode) calcd 4102.9, found 4103.9.

Peptide Conjugate 2.

To a solution containing the derivative **7** (16 mg, 9.7 µmol) in 1 mL of H_2O/acetonitrile (1:1) was added the peptide **9** (34 mg, 43 µmol). The reaction mixture was stirred for 6 h at 25 °C. Conjugate **2** was isolated after purification by RP-HPLC as a white powder (12 mg, 2.9 µmol, 30%). Mass spectrum (ES-MS, positive mode) calcd 4161.7, found 4160.3.

QCM-D measurements.

Quartz crystal microbalance is a mass sensitive method based on the piezoelectric properties of quartz crystal. QCM-D measurements were performed using Q-Sense D300 and E1-E4 instruments (Q-Sense, AB, Göteborg, Sweden) equipped with axial flow chamber (D300) and one (E1) or four (E4) laminar flow chambers and polished AT-cut piezoelectric quartz crystals (diam.14 mm) covered by a 100 nm thick gold layer (QSX 301–Q-Sense). Besides measurements of bound mass related to changes in the resonance frequency *f*, of the piezoelectric sensor resonator, the QCM-D technique also provides structural information of the biomolecular films *via* changes in the damping *D* (energy dissipation) of the oscillator. In the case of cell adhesion monitoring, the obtained responses provide proper signatures for attachment and spreading of the cells on the functionalized crystal resonator. *f* and *D* were measured at the fundamental resonance frequency (5 MHz) as well as at the third, fifth, seventh, ninth, eleventh, and thirteenth overtones (n = 3, 5, 7, 9, 11 and 13).

Experiments were conducted either in a continuous flow of buffer with a flow rate of 50 µL/min by using a peristaltic pump (ISM935C, Ismatec, Zurich, Switzerland) or using open modules (Q-Sense) for static mode**.** For the latter case, the signals were stabilized with 1 mL buffer solution and small volumes of protein, ligand or cell suspensions were injected during the measurement. The temperature of the E1-E4 QCM-D platforms and all solutions were stabilized (*via* an Ependorf Thermomixer) to ensure stable operations at 37°C for the building of the biomolecular assembly and also for the cell adhesion assays. All buffers were previously degassed in order to avoid bubble formation in the QCM-D measuring chamber.

In the case of homogeneous, quasi-rigid films (for which $\Delta D_n/(-\Delta f_n/n) << 4 \times 10^{-7}$ Hz^{-1} for a 5 MHz crystal), the frequency shifts are proportional to the Δm mass uptake per unit area that can be deduced from the Sauerbrey relationship (1):

$$\Delta m = -C\,\Delta f_n/n \qquad (1)$$

where the mass sensitivity, C, is equal to 17.7 ng cm^{-2} Hz^{-1} at f_1 = 5 MHz.

Prior to use, the gold-coated crystals sensors (Q-Sense QSX 301) were exposed to a UV-ozone treatment for 10 min using UV-Ozone cleaner (Jelight Company) and immersed in ethanol under stirring during 20 min. The surfaces were then dried under nitrogen before dipping overnight in the mixture comprising 1mM ethanol solution of thiols (EG_6Biot:EG_4OH of known ratio), then carefully rinsed with ethanol and dried with nitrogen. The functionalized gold quartz crystal was then mounted in the QCM-D flow module and the formation of the biomolecular layer was monitored in the presence of PBS buffer as the running buffer. The transducer surface was then exposed subsequently to 50 $\mu g.mL^{-1}$ streptavidin solution (in PBS) and after rinsing with 1 µM (or 0.1 µM for low surface coverage) of biotinylated cyclodecapeptide scaffold. The resulting functionalized-surface was rinsed under flow until reaching the stabilization of the QCM-D signals. The resulting biomolecular assembly will denoted SAM-EG_6Biot(x%)/SA/**1** (or **2**).

For cell-adhesion assays, the quartz crystals sensors were equilibrated in the QCM-D measurement chamber with DMEM medium (without serum) at 37°C. *f* and *D* were recorded continuously during the incubation (using a flow rate of 100 µL/min) of the cells (100 000 cells/mL) suspended in the same medium until reaching stable signals. Then the measurement chambers were rinsed with DMEM medium (without serum) and the spreading of the cells on the resonator surface was monitored by the changes in *f* and D.

Microscopy experiments coupled with QCM-D were performed using the Q-Sense window module 401 (Q-Sense AB, Göteborg, Sweden) and a microscope Axio Imager A1m

(Carl Zeiss S.A.S., France). The images were registered and treated using the software Axiovision from Carl Zeiss S.A.S.

Electrochemical experiments.

Cyclic voltammetry experiments were performed with a conventional three-electrode potentiostatic system. The equipment was a CHI 440 model potentiostat (CH-Instruments). Electrode potentials were referred to an Ag/AgCl/KCl (3M) as reference. The counter electrode was platinum and the working electrode was gold quartz sensors activated and functionalized as described previously. The electrochemical cell was home-made, the working electrode being at the base of the cell covered by the electrolyte solution in which the counter and the reference electrodes were immersed. The compactness of the thiolate layer was determined using FcMeOH as a soluble redox probe (5.10^{-4} M in KPF_6 or in Na_2SO_4 or in phosphate buffer solutions at 0.1 M). Electrochemical reductive desorption experiments were conducted in NaOH 0.5 M degassed aqueous solution.

Preparation of template-Stripped Gold (TSG)

TSG substrates were prepared using commercially available (Ssens, Netherlands) slides of mica, onto which a ~200nm thick gold was deposited. The gold side of the slide was then glued to an appropriately sized glass slide (after cleaning with Piranha solution) using EPO-TEK 377 and cured for 90 min at 150°C. After cooling, the slides were detached from mica by immersion in freshly purified (by distillation) THF and used immediately for the adsorption of the SAM.

AFM imaging.

The AFM experiments were performed with an Agilent PicoPlus AFM microscope (Scientec, France) in a home-made liquid cell. The images were recorded in phosphate buffer (pH 7). The tips used for imaging the surfaces are Hydra2R-100N from AppNano (nominal spring constant 0.011 $N.m^{-1}$, resonance frequency 21 kHz). The TSG substrates were functionalized without pre-treatment using the same procedure than that used for gold-coated quartz crystal. The TSG substrates were imaged in tapping mode in order to limit the contact between the tip and the substrate and protect the biomolecular assembly. The instrument was calibrated with a specific surface (TGQ1 from NT-MDT). The images were recorded at 1 Hz and with size 3 x 3 µm, 1 x 1 µm, 0.5 x 0.5 µm or 0.25 x 0.25 µm. All the images were treated using Gwyddion and analysed with SPIP (Image Metrology) software.

Cell culture.

HEK293(β_3) and HEK293(β_1) are subclones of the human embryonic kidney HEK293 cell line, stably transfected by a plasmid encoding respectively the human β_3 or the human β_1. Cells were cultured as adherent monolayers in DMEM (Dulbecco's Modified Eagle's Medium) enriched with 4.5 $g.L^{-1}$ glucose and supplemented with 1 % glutamine, 10 % FBS (Fetal bovine serum), penicillin (50 $U.mL^{-1}$), streptomycin (50 $\mu g.mL^{-1}$) and G418 (700 $\mu g.mL^{-1}$). All cells were maintained at 37°C under an atmosphere of 5 % CO_2. After washing with PBS, cells were detached from the plate using Trypsin (Gibco). After counting and centrifugation, the cells were re-suspended (without serum) in DMEM at the interest concentration of 100 000 cells/mL.

Results and Discussion

Molecular design of the peptides.

Based on previous results,[8,9] we reasoned that a tetrameric RGD-containing template would be suitable for specific targeting of tumor cells. For instance, we have shown that this tetrameric RGD peptide was more efficient than its monovalent homologue.[28] In this context, two compounds **1** and **2** were designed and prepared as described in scheme 1. Briefly, the removal of alloc and boc groups from cyclodecapeptide **3** permitted the respective anchoring of biotin and aminooxy functions providing the key intermediate **7**. Finally, the compounds **1** and **2** were obtained *via* the respective oxime ligation of RGD peptide **8** or nonsense RβAD peptide **9**. All compounds were characterized by ES-MS analyses (See the supplementary information).

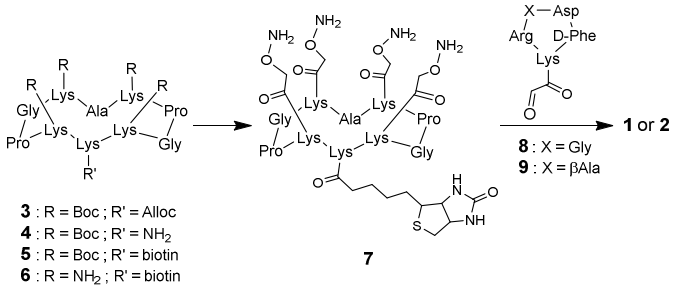

Scheme 1 Synthesis of compounds **1** and **2**

SAM formation and structural characterization.

Self-assembled monolayers (SAMs) of alkanethiols on gold are commonly used to immobilize biomolecules on surface. Whitesides *et al.*[29] demonstrated that alkanethiolates terminated with oligo(ethyleneglycol) (OEG) moieties form bioinert SAMs and confer to the monolayer a resistance to non-specific protein adsorption. The approach used here to immobilize RGD clusters involved biotin-streptavidin bio-specific interactions allowing the control over orientation and density of the subsequent attached compound **1**. Streptavidin (SA) conjugation on biotinylated functionalized-SAMs has been extensively studied

by a number of research groups.[29-33] Regarding the mixed SAMs formed from the self-assembly of biotin and hydroxy-terminated thiols, the influence of the molar ratio biotin-thiol/diluent thiol on the SA binding capacities depends on the structural properties of SAMs such as alkylchain length, presence of OEG-terminated long alkyl chain or amide group containing alkanethiols. Electrochemical techniques and QCM can provide information on the structural characterization of the mixed SAMs. In order to control the SA surface coverage, we studied the structural characterization of the SAMs. We have previously reported characterizations of pure and mixed SAMs formed from EG_4OH and azide functionalized OEG alkanethiol (EG_6N_3) adsorbed onto gold surface using these techniques.[34] QCM-D has also been involved in the monitoring of the mixed SAMs building. Electrochemical responses of redox probes diffusing through the SAMs give information on the molecular organization of the monolayer. We demonstrated in particular that the SAM formed from pure EG_4OH is densely packed and well organized. In the present work, we study the structural properties of the mixed SAMs formed from EG_4OH and EG_6Biot with the objective of investigating the influence of the EG_6Biot introduction in the pure EG_4OH SAM. An acoustical mass of 280±50 ng cm^{-2} was extracted from the QCM-D profile, characterizing the formation of a mixed SAM prepared by the adsorption of a 50:50 mixture of each thiol (SI-Fig. S1). This mass uptake has been compared to those measured on SAMs formed from pure EG_4OH or pure EG_6Biot (table 1). The data from table 1 show an increase in mass uptake as a function of increasing EG_6Biot molar fraction. This can be interpreted by the increase of biotinylated alkanethiolate adsorbed on gold surface owing to the difference in molecular weights (EG_6Biot MW= 694 $g.mol^{-1}$ and EG_4OH MW = 380 $g.mol^{-1}$).

Table 1: SAMs Structural Characterizations

$x_{(EG)6Biot}$	m_{QCM} ng/cm^2	Γ_{Au-SR} (QCM)[a] (10^{-10}mol cm^{-2})	Epc (V*vs.*AgCl/Ag)	Fwhm (mV)	Γ_{Au-SR} (RD)[b] (10^{-10}mol cm^{-2})
0	230±40	(6.0 ± 1.0)	-1.05 ± 0.02	37 ± 4	(6.6 ± 0.7)
0.50	280±50	/	-1.03 ± 0.03	38 ± 3	/
1	347±80	(5.0 ± 1.2)	-1.04 ± 0.03	41 ± 2	(4.9 ± 0.8)

[a] Obtained from QCM-D experiment and assuming a negligible contribution of the solvent to mass uptake

[b] Obtained from electrochemical reductive desorption experiment.

In order to refine the QCM-D determination, electrochemical reductive desorption of SAMs was investigated at a basic pH. The reductive desorption process implies cleavage of the metal-sulfur bond and formation of the corresponding thiolate:

$$R\text{-}S\text{-}Au + e^- \rightarrow R\text{-}S^- + Au \quad (1)$$

Table 1 compares the reductive desorption parameters corresponding to single-component SAMs prepared from EG_4OH or EG_6Biot with mixed SAMs containing 50% of EG_6Biot. The process is characterized by a sharp cyclic voltammogramm (CV) cathodic stripping peak at a potential close to -1V (SI Fig. S2, S3). The underlying area of the peak is related to the alkanethiol surface coverage. The desorption potential that is known to be a function of the alkylchain length was similar for the three cases studied (Table 1). The very small full width at half-maximum fwhm (table 1) has been interpreted to be the result of interchain attractive interactions between Van-der-Waals contacting molecules.[35] The peak width of the biotinylated single-component SAM is broader than that of the hydroxylated single-component SAM. This result is attributed to packing constraints imposed by the bulky biotin end groups. The charge associated with the electrode reaction equals 62.7 ± 6 $\mu C.cm^{-2}$ (for SAM of pure EG_4OH) which corresponds to a thiolate surface coverage of Γ = (6.6 ± 0.7) 10^{-10} $mol.cm^{-2}$ (mean ± SD over 5 experiments) and a molecular area for the alkanethiol EG_4OH of 27.7 $Å^2$. This value is in accordance with previous data reported in the literature by Zheng *et al.*[36] who calculated a molecular area of the alkanethiol EG_4OH of 27.4 $Å^2$/chain considering that the resulting self-assembled monolayer has a helical configuration. The surface concentration of thiolate in the biotinylated single-component SAMs is lower than that of the hydroxylated single-component SAM, corresponding to a molecular area of 31.8 $Å^2$. We noticed that the mixed SAMs prepared with a molar fraction of 0.50 EG_6Biot exhibit similar characteristic parameters as those of the single-component hydroxylated SAMs. We can also compare this thiolate surface coverage with the values obtained by QCM-D during the formation of SAMs. QCM measures the organic mass together with solvent trapped between the adsorbed molecules. In the case of EG_4OH and EG_6Biot SAMs (Table 1), as we obtain similar surface densities from the two techniques we could conclude that the contribution of solvent acoustically coupled to the SAMs is negligible. In addition, we explain the lower surface density for EG_6Biot compared to that obtained for EG_4OH by the packing constraints imposed by the bulky biotin end groups.

We have previously demonstrated, by using cyclic voltammetry (CV) of reversible redox probes that SAMs formed on gold substrate from EG_4OH lead to a rather closed monolayer structure of the SAMs.[34] In order to complete the molecular organization of mixed SAMs formed with pure EG_6Biot, we studied the CV responses of the reversible redox probe ferrocenemethanol (FcMeOH). SAMs prepared from pure EG_4OH or pure EG_6Biot solutions exhibit similar trends confirming that the EG_6Biot form well-ordered SAMs and that it partially blocks faradaic reactions (SI Fig. S4). In addition the electron transfer process of the FcMeOH oxidation has been quantitatively characterized by the determination of the apparent rate-limiting electron transfer constants k° from Tafel plots (SI, Figure S5). As k°(EG_4OH) = 4.1 10^{-5} $cm.s^{-1}$ and

k°(EG_6Biot) = 3.3 10^{-4} cm.s^{-1}, EG_6Biot appears to be a more open monolayer. We notice that these values are considerably lower than the standard transfer rate constant of FcMeOH calculated[37] at a bare Au electrode (k° = 0.19 cm.s^{-1}). Assuming that electron transfer can only occur on bare gold resulting from defaults in the SAM, these results demonstrate that the SAMs involved in this work exhibit a compactly packed state with almost a low amount of defects.

Binding of streptavidin to biotin-terminated SAM.

The immobilization of streptavidin (SA) onto mixed biotinylated SAMs was monitored by QCM-D. The loading capacities of SA were examined as a function of the molar fraction of EG_6Biot in the incubation solution of thiols. It relies on a fine balance between the density of biotin tail on the SAM surface, their accessibility and the steric hindrance of SA protein. The structural characterization of the SAMs shows similar properties for those prepared from single-component as for mixed SAMs. Taking into account the similarities of the chemical structure of the two alkanethiols involved in this study, which suggests comparable adsorption kinetics, we assume in a first approximation that the composition of the SAMs on gold surface reflects the composition of the incubation solution of thiols.[38] The absence of amide group between the long alkyl chain and ethylene glycol spacer (OEG) that could induce laterally interacting amide group *via* hydrogen bond could not lead to phase segregate on the gold surface. We can thus make the assumption that the two components with biotin and hydroxyl-terminated thiols are assembled in a random distribution without phase segregation.

A typical QCM-D profile for the construction of the biomolecular assembly (SA/**1**) on mixed SAM containing 10% of EG_6Biot is shown in figure 2.

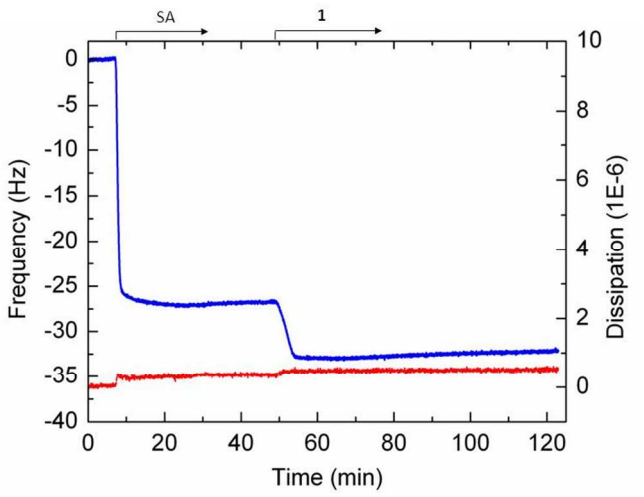

Fig. 2 QCM-D profile (shifts in resonant frequency (blue curve) and in dissipation (red curve) *vs.* time) illustrating the building of the biomolecular assembly SA/**1** on SAM-Biot prepared with 10 % of EG_6Biot (7th overtone data).

The signal at the beginning of the adsorption process corresponds to the baseline from pure PBS buffer flowing on a quartz crystal recovered with a mixed SAM prior to protein injection. As a result of the SA incubation and adsorption, the frequency drop is 25 ± 2 Hz and the change in dissipation factor appears very low (less than 0.2 × 10^{-6}). By using the Sauerbrey relation, valid for thin and rigid layers, this shift in frequency can be converted to SA mass uptake taking into account that the QCM measurements include the water that is hydrodynamically coupled to the adsorbed protein (Δm_{QCM} = 442 ± 35 ng/cm^2). This value is in good agreement with the QCM-D reported results for SA layer adsorbed on biotinylated SAMs.[33]

The evolution of the binding capacities as a function of the biotin thiol molar fraction in the incubation solution is depicted in figure 3. The maximum loading capacity is reached near 10% which remains quasi-constant on further increase of the biotin thiol fraction

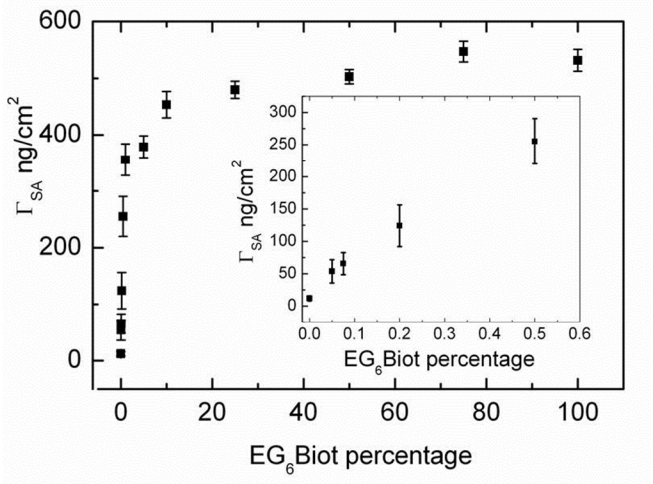

Fig. 3 Plot of SA Sauerbrey mass vs. percentage of EG_6Biot in the thiols mixture used to prepare the biotinylated SAM. Insert: Plot illustrating the lower percentages.

The optimum binding capacity of 10 mol % is consistent with most of the reported results in literature.[30-32] In contrast, some authors showed a decrease of the adsorbed SA above the maximum. They interpreted this reduced SA binding by the lack of accessibility of the biotin tails on the SAM surface due to sterical hindrance between two adjacent biotin groups or by the lack of protruding biotin head group. Nelson *et al.*[31c] demonstrated that pure biotin-terminated alkanethiol SAMs are poorly ordered and do not show appreciable orientation of biotin headgroups. It is worthwhile to mention that the molecular system involved in our work is not exactly the same than those reported in literature. The electrochemical investigations of the single-component EG_4OH and EG_6Biot SAM permeabilities proved to be comparable suggesting ordered states with protruding biotin head groups exposed to the solution even in the case of rich-biotin monolayer. The

difference in the structural architecture could be ascribed to the chemical structure of the two alkanethiol components but also to microscopic and nanoscopic gold surface state.

As QCM is sensitive to both bound organic molecules and hydrodynamically coupled water, and considering a degree of hydration of 50% that has been reported in the literature[33] for a densely packed 2D arrangement of SA, a surface density of molecules around 2.2 × 10^{12} molecules cm^{-2} can be estimated (using a molecular weight of 60 kDa).

The SA platform on the transducer surface was then used to anchor the biotinylated cyclodecapetide scaffold **1** bearing four RGD motifs. Incubation of 1 µM **1** solution leads to a decrease in frequency and to a small increase in dissipation until reaching saturated binding and stable signals (Figure 2). After rinsing with buffer, the final shifts in frequency Δf and dissipation ΔD were found to be $\Delta f = -5.8 \pm 0.8$ Hz and $\Delta D = 0.2 \pm 0.1 \times 10^{-6}$. As $\Delta D_n/(-\Delta f_n/_n)$ value is lower than 4×10^{-7} Hz^{-1} the Sauerbrey approximation can be used to calculate the mass of the **1** layer: 103 ± 14 ng cm^{-2}.[39] Making the assumption of hydration ratio of 50% to the **1** layer, a surface density of 7.5 10^{12} molecules.cm^{-2} can be estimated. The latter estimated high surface density seems to indicate a molecular **1**:SA ratio of 2. This result is reinforced by the comparison of the dimension of each biomolecule: the projected surface area of **1** molecule was determined to be close to 9 nm^2 (ESI) and 25 nm^2 for SA.

The lowest percentage of bound biotinylated thiol (0.05%) leads to the lowest SA coverage (45.8 ± 9 ng.cm^{-2}). This result can be compared to that corresponding to the non-specific adsorption of SA onto SAMs without biotin-terminated groups, for which very low surface coverage of SA was adsorbed (11.5 ± 2 ng.cm^{-2}) (SI, Fig. S6). Such low amount is attributed to the non-fouling properties of the PEGylated surface. We noticed that in a first stage, SA was adsorbed with a higher amount on the PEGylated surface but more than the half was released during the rinsing step (ESI, Fig. S7). SAMs prepared with low EG_6Biot surface coverage (lower than 1% of EG_6Biot in the alkanethiols mixture) showed identical behaviour. For higher surface coverage, a negligible release was observed during the rinsing step. Taking into account the difference of SA mass uptake between 0 % and 0.05 %, we can conclude that the binding of SA on a 0.05 % EG_6Biot surface is mainly of specific nature. Regarding the high distance separating the biotin sites on the diluted biotinylated SAM surface, one part of SA could be bind by only one biotin-binding SA pocket whereas a small fraction is immobilized on the SAM surface by non-specific adsorption. Under such conditions, SA can be desorbed partially upon exposure of the functionalized surface to biotinylated molecule as it has been shown by Jung and coworkers.[31b] This phenomenon was observed for SA-SAM displaying a low surface coverage (EG_6Biot below 0.1%) when a solution containing 0.1 µM **1** was introduced on the surface. A partial desorption of SA was observed as shown by the QCM-D profile (Fig. S7). After a first drop in frequency corresponding to the adsorption of **1**, the frequency increases before stabilizing to a level corresponding to a final shift in frequency of -1.6 ± 0.2 Hz (measured after rinsing). Under such conditions and by taking into account the undetectable mass uptake for the expected adsorption of **1**, one can estimate a remaining hydrated SA surface coverage of 28.3 ng.cm^{-2} (using Sauerbrey equation). Regarding the hydration degree of such diluted protein layer, a linear relationship between the relative contribution of coupled water to the frequency response and the surface coverage for globular protein has been reported.[40] Thus, it has been demonstrated by using a phenomenological model that the hydration degree decreases on increasing protein surface coverage. In the case of very low surface coverage corresponding to the present SA diluted surface, a hydration degree close to 80% has been determined.[40] Using the assumption of a hydration ratio of 80% for this protein layer, a density of 5.7 × 10^{10} molecules.cm^{-2} can be calculated from which we can also estimate the intermolecular spacing of adhesive cluster (consisting of one SA with two compound **1** molecules) on the SAM surface. Thus, as each EG_6Biot binds one SA, we can make the assumption that the average distance between each adhesive cluster is closed to 22 nm for a mixed SAM containing 0.05% of EG_6Biot in the mixed SAM.

In order to reinforce this hypothesis, we performed AFM images under tapping mode of SA-functionalized surfaces for low surface coverage ranging from 0.05 to 0.2% of EG_6Biot (Figure 4).

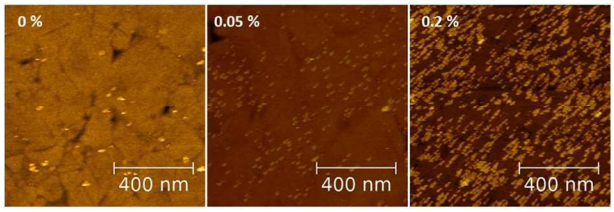

Fig. 4 Tapping AFM images of biotinylated SAMs (formed from thiols mixture containing 0, 0.05 or 0.2% of EG_6Biot) after the adsorption of streptavidin. Images display a surface area of 1.0 µm x 1.0 µm (horizontal scale bars 400 nm). The average height of the biomolecular layer is closed to 6 nm (Fig. S8).

The AFM images were used as a qualitative tool to address the distribution of the proteins on the surface and also to determine the density of SA on the functionalized-SAM surfaces for 0.05%. After incubation of SA onto biotinylated SAMs, the AFM images presented on figure 4 in the case of SAMs prepared from thiol mixtures of 0.05% and 0.2% of EG_6Biot clearly show a homogeneous distribution of spots corresponding to the adsorbed protein on the surface. The AFM images confirm that SA density increases with increasing biotin groups on mixed SAMs (Fig. 4). The density of protein adsorbed on the surface was determined by counting the spots on each image using AxioVision software. We determined a value of 8.3 ± 2 ×10^{10} proteins.cm^{-2}. This value is in agreement with the data determined by using the QCM-D data considering a hydration ratio of 80%.

Monitoring cell adhesion by QCM-D.

In the present study, we investigated the initial adhesion of human embryonic kidney cells HEK293 (β3) that overexpress

$\alpha_v\beta_3$ integrin onto surfaces functionalized with the macromolecule **1** by using the QCM-D technique. It has been shown that QCM-D is a well-suited technique for real-time acquisition of cell response.[17,18] As the decay length of the shear wave (about 250 nm for 5 MHz) is assumed to be less than the cell diameter (about 10 µm), this suggests that QCM-D probes the lower part of the cells close to the cell-substrate interface giving very high sensitivity to processes limited to the region where the actual adhesion occurs.[17] The penetration depth of the damped wave coupled to the resonator can be influenced by the viscosity, stiffness and shape of the attached cells, which in turn affects the QCM-D signals. Several groups demonstrated that the adhesion of cells onto the resonator surface induces a shift in frequency that scales linearly with the fraction of the surface covered with the cells. For example Foss and coworkers[20] previously noted that decreases in *f* (and increases in *D*) correlate with an increase in the number of adhered cells and an increase in the proportion of the surface covered by cells. The shift in dissipation reflects changes in overall cell rigidity which is correlated to the spreading of the cells. Our group reported the analysis of cell-adhesion process on RGD-functionalized supported lipid bilayers by coupling QCM-D with optical microscopy aiming to determine the thresholds for cell attachment and cell spreading.[9b] These QCM-D experiments were achieved in the cell culture medium (DMEM) without serum and the time course of the adhesion assays does not exceed three hours in order to avoid cells secretion of endogeneous extracellular membrane (ECM). Shortening the time scale of the experiment ensures the characterization of the interactions between cells and compound **1** functionalized surface.

We first evaluated the cell adhesion on sensing surfaces presenting 10% of EG_6Biot in the SAM which corresponds to a saturated layer of SA (Figure 5). The pure SAM-EG_4OH functionalized sensor proves to be insensitive to the cells just seeded on the surface, as depicted by the flat QCM-D profile. It is well known that the QCM-D technique does not sense the mass increase from cells that simply settle on the surface.[41] The cells have to be firmly attached onto the quartz surface to the substratum to exert their influence on the shear oscillation of the quartz resonator, the sole presence of the cellular body in close vicinity with the quartz surface is barely detectable. In return, the presence of RGD ligand on the surface of SAM-EG_6Biot(10%)/SA/**1** promotes the cell adhesion as demonstrated by the initial decrease in *f* and an increase in *D* (Figure 5) as the cells attach to the functionalized resonator surface. After approximately 40 min cell incubation both Δf and ΔD reaches quasi-stable values that remain unchanged after rinsing with DMEM medium. The rinsing step with DMEM medium does not induce cell release as shown by the stable *f* and *D* signals. This observation proves that the cells are firmly attached to the resonator surface.

As the cyclic RGD peptide is known to interact with high affinity to the $\alpha_v\beta_3$ integrin, we compared the cell adhesion process of HEK293 (β_3) cells on two surfaces displaying either RGD (compound **1**) or RβAD (compound **2**) peptides (SI, Fig. S9). The RβAD sequence (Arg-βAla-Asp) has been shown to exhibit lower affinity for the $\alpha_v\beta_3$ expression of eukaryotic cells.[42,43]

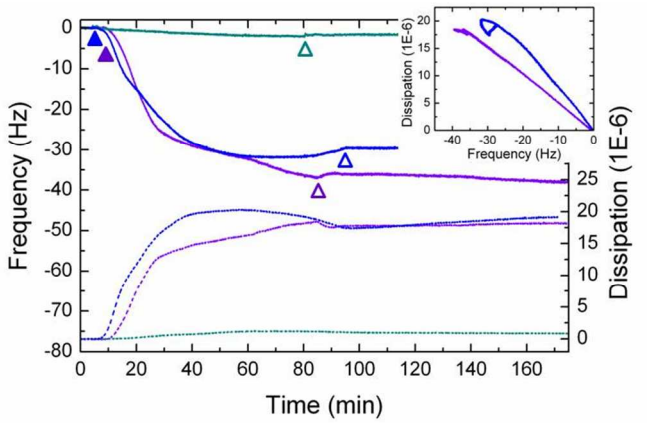

Fig. 5 QCM-D profiles illustrating the cell adhesion for HEK293 (β_3) cells (100 000 cells/mL) flowing either, on SAM-EG_4OH (turquoise blue), on SAM-EG_6Biot(10%)/SA/**1** (violet) or on SAM-EG_6Biot(10%)/SA/**2** (blue). Frequency changes were presented as solid lines and dissipation as dashed lines. Insert: *D* vs. *f* plot of HEK293 (β_3) cells flowing onto the two different functionalized surfaces (SAM-EG_6Biot(10%)/SA/**1** (violet) and (SAM-EG_6Biot(10%)/SA/**2** (blue). The cellular medium is DMEM without serum. For clarity, only the 7th overtone is presented. The arrows indicate the time of injections (full: cells and empty: rinsing with DMEM).

The response of HEK293 β_3 cells onto a functionalized surface saturated with RβAD is illustrated on figure 5. The signature of HEK β_3 on the two functionalized surfaces exhibiting RGD and RβAD peptides are identical. We deduce that those saturated surfaces (compound **1** or **2** adsorbed on SAM-EG_6Biot(10%)/SA) promote the adhesion of HEK293 (β_3). In order to gain more insights of the adhesion process on such adhesive substrates, the signals were shown as *D-f* plot where dissipation is plotted as a function of the frequency. This is an alternative representation of the QCM adhesion data, where time is implicit and used to derive information about cell attachment to substrate. Such representation is often used as a fingerprint of the cell adhesion process, since the lateral sensitivity of both the resonant frequency Δf and dissipation factor ΔD is the same.[17] A plot of ΔD versus Δf is qualitatively independent of the spatial distribution of the cells on the surface. The insert of figure 5 illustrates the *D-f* plots for cells adhered on SAM-EG_6Biot(10%)/SA/**1** and SAM-EG_6Biot(10%)/SA/**2**. The extent of *f* and *D* changes are similar for RGD and RβAD-functionalized surfaces. The *D-f* plots were essentially linear with corresponding slopes of $-0.52 \pm 0.04 \times 10^{-6}$ s for adhesive RGD surface and $-0.76 \pm 0.08 \times 10^{-6}$ s for RβAD surface. The unexpected response of the HEK293 (β_3) cells onto the theoretical non-sensing surface SAM-EG_6Biot (10%)/SA/**2** could be explained by the non-specific binding of the cells attributed to electrostatic interactions between cells and RβAD-containing surface.[44] As the $\Delta D/-\Delta f$ ratio represents the energy loss per unit of attached mass, the ratio reflects the spreading of the cells. The higher is the

spreading, the lower is the slope. The lower $\Delta D/-\Delta f$ slope on RGD surface (0.52×10^{-6} s) can be ascribed to a more rigid layer coupled to the resonator. The higher *D-f* slope observed for cells seeded on RβAD surface characterizes a more dissipative film because of lower cell spread cells. Rodahl *et al.*[45] demonstrated that a more rigid and compact mass is expected to yield a small $\Delta D/\Delta f$.

In order to improve the specificity of the RGD-functionalized surface and to discriminate the cellular responses between RGD and RβAD surface, the adhesion process was investigated at lower surface coverage: 0.5 %, 0.075 % (Fig. S10) and 0.05 % (Fig. 6). The decrease in peptide motifs was achieved by varying the molar ratio of EG_6Biot in the mixture used to prepare the SAM.

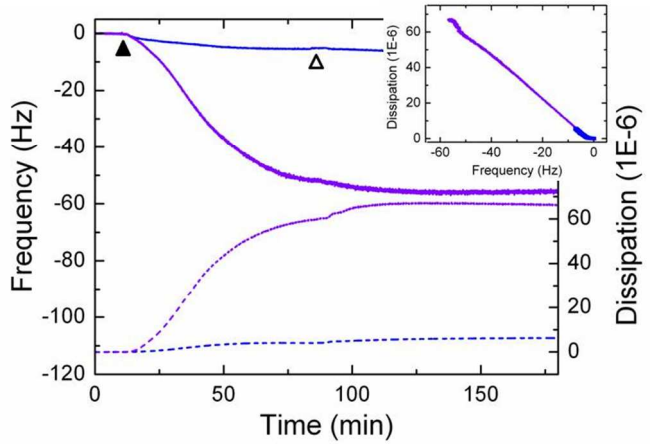

Fig. 6 QCM-D profiles characterizing the adhesion of HEK293 (β_3) on quartz crystals functionalized with SAM-EG_6Biot(0.05%)/SA/**1** (violet) or SAM-EG_6Biot(0.05%)/SA/**2** (blue). Frequency changes were presented as solid lines and dissipation as dashed lines. Insert) D vs. *f* plots illustrating the interaction of HEK293 (β_3) cells with the functionalized surfaces (SAM-EG_6Biot(0.05%)/SA/**1** in violet and pink) and (SAM-EG_6Biot(0.05%)/SA/**2** (in blue). For clarity, only the 7th overtone is presented. The arrows indicate the time of injection (full: cells and empty: rinsing with DMEM).

The QCM-D profiles in figure 6 illustrates the adhesive properties of **1** in comparison with surface displaying **2** on lower SA grafted density (0.05%). Significant higher shifts in frequency and dissipation were recorded for RGD surface. The response on RβAD surface does not exceed 14% of the maximum frequency shift and 9% of the maximum dissipation changes relative to RGD surface. This is reflected in the *D-f* plot by the extent of *D* and *f* variation which is very limited for RβAD (Insert of figure 6). On decreasing the surface from 10 % to 0.05 % through 0.5 % the extent of *D* and *f* variations for RGD surface did not change drastically while gradual changes were observed for RβAD surface (SI-Fig. S10). This result can be interpreted by the gradual decrease in the number of cells attached to the RβAD surface compared to RGD surface. It agrees well with the work of Wegener *et al.*[46] reporting that the more cells are attached to the resonator surface, the bigger is the resulting shift in resonant frequency. Such evolution has been assessed for experiments performed by increasing the number of HEK293 (β3) cells seeded on adhesive RGD surfaces. A regular decrease in *f* and increase in D was recorded during an increase of seeded cells (Fig. S11). Regarding the $\Delta D/-\Delta f$ ratio measured on the diluted RGD surface (0.05%), we noticed a significant increase of the slope from 0.52×10^{-6} s (for 10%) to 1.32×10^{-6} s (for 0.05%). The higher slope measured on the diluted RGD surface compared to the saturated one can be ascribed to lower cell layer rigidity. Decreasing the RGD peptide ligand surface density leads to a decrease in the interaction of cells with the resonator surface resulting in reduced cell spreading which corresponds to a softer adlayer. Between 10% and 0.05%, two additional percentages were investigated, $\Delta D/-\Delta f$ slope of $0.57 \pm 0.06 \times 10^{-6}$ s and $1.22 \pm 0.02 \times 10^{-6}$ s were obtained for 0.5 % and 0.075 % respectively (SI Fig.S10). The result obtained with 0.5% is similar to that obtained for 10%, while for 0.075% the $\Delta D/-\Delta f$ ratio is closed to that measured with 0.05% on RGD-functionalized surface. These observations demonstrate that decreasing the density of non-sense peptide **2** induces a lowering of the non-specific interactions of the HEK β_3 cells with the functionalized surface. In contrast, a diluted RGD surface keeps high affinity for cell targeting. We conclude that the decrease in RGD surface density improves the selectivity of the surface displaying RGD *versus* RβAD surface.

Whitesides *et al.*[4a] demonstrated that the number of endothelial cells adherent to mixed SAM-RGD is dependent on the mole fraction of RGD-alkanethiol present in the solution for the preparation of the mixed SAM. The groups of Kessler and Spatz[47] also showed that the number of attached cells is clearly related to the RGD surface density. They reported that cell attachment as a function of RGD concentration shows a sigmoidal increase indicating that there is a critical minimum density for cell response. They determined critical ligand spacings above which cell attachment and cell spreading were highly restricted. They showed that by using nanogold-anchored RGD peptides surfaces with a lateral spacing of 58 nm (corresponding to a RGD density of 500 molecules/μm^2) or less is essential for focal adhesion formation, but an RGD intermolecular spacing of 85 nm was sufficient for cell attachment. Hudalla *et al.*[48] determined a 11 nm spacing between RGD covalently linked to SAM for stem cell spreading and 36 nm for cell attachment. Massia *et al.*[49] reported a minimum ligand spacing surface of 440 nm for spreading and 140 nm for focal contact formation. We have previously reported a critical interligand RGD spacing of 80 nm for cell attachment on RGD-functionalized supported lipid bilayers when an RGD spacing of 10 nm was necessary to observe cell spreading on fluid membrane.[9b] The discrepancies between these results focused on the threshold ligand spacing depend on different factors such as the particular RGD ligand molecule used in each study (linear or cyclic RGD), ligands clustering or single ligand presentation and cells type.

In the present work, the QCM-D signals indicate a difference in cell spreading assessed by the difference in $\Delta D/-\Delta f$ slopes from a diluted RGD surface (0.05 %) to a saturated one (10 %). Based on our previous calculation of SA surface densities (determined from the average values extracted from

QCM-D considering an hydration ratio of 80% for the diluted SA surface and the SA density determined by AFM imaging of low surface density), the resulting peptide densities for 0.05% corresponds to an average surface density of 700 RGD clusters molecules.μm^{-2} (consisting in one SA bearing two compounds **1**, average lateral spacing of 38.5 nm), whereas for 10%, 45 000 molecules.μm^{-2} (average lateral spacing of 5 nm) can be estimated. The interligand spacing of 39 nm represents the optimized distance between two RGD clusters (formed by the binding of two compounds **1** on one SA) allowing the selective adhesion of HEK293 (β_3) cells.

However it should be difficult to give a threshold cluster spacing for cell adhesion and spreading on SAM-EG_6Biot/SA/**1**. Such evaluation is indeed limited by the detection limit of QCM-D technique for cell seeding. If the peptides grafting density decreases to an extreme low extent, it would induce a great decrease in the amount of attached cells and in such a case, as the proportion of the surface covered by the cells will be much smaller than the uncovered surface, the cells would not be detected.

Additionally, we performed a controlled experiment with cell line HEK293 (β_1) expressing $\alpha_v\beta_1$ integrin that is known to exhibit a lower affinity for the RGD peptide sequence.[50] To this end, we examined the QCM-D response of HEK293 (β_1) on functionalized surfaces prepared from 10% and 0.05% EG_6Biot. We did not observe a significant difference for the adhesion of the two cell lines β1 and β3 on SAM-EG_6Biot(10%)/SA/**1** (Figures S12 and S13). Conversely, on SAM-EG_6Biot(0.05%)/SA/**1**, the QCM-D experiment reveals a significant difference of adhesion between the HEK293 (β_1) and (β_3) (SI, Fig. S14). The maximum response in frequency of HEK293 (β1) does not exceed 18 ± 2 % of the frequency shift measured with HEK293 (β3). Regarding the dissipation changes upon interaction of (β1) with the RGD functionalized surface, it represents only 19 ± 4 % of the maximum dissipation changes relative to (β3) (these percentages have been calculated by the average of experiments carried out in static and in flow mode). This result provides a new insight on the specificity of the diluted RGD functionalized surface: SAM-EG_6Biot(0.05%)/SA/**1**.

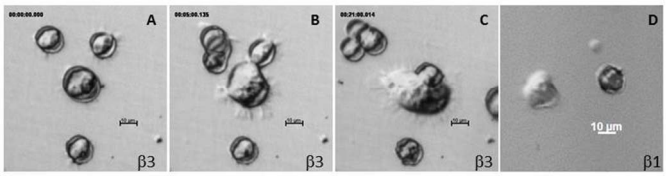

Fig. 7 Optical microscopy images (DIC measurement) of HEK293 (β_3) adherent cells (A, B, C) and HEK (β1) non-adherent cells (D) on SAM-EG_6Biot (0.05 %)/SA/**1** substrates (quartz crystal resonator) being captured during QCM-D experiment. (A) t = 0, taken at the beginning of the attachment of the cells; (B) t = 5 min and (C) t= 21 min. During this time of observation some additional cells were seeded on the area of interest. Scale bar = 10 µm. Cell suspension (100 000 cell/mL) was continuously injected for 25 min at 100 µL/min.

In order to assess the HEK293 (β_3) cells spreading for low grafting densities, we monitored the morphological changes in the projected area of cells adhering on the sensing SAM platform prepared from 0.05% EG_6Biot. From the images of live cells in figure 7, we observed a fast spreading of the adhering cells (See also movie picture available in the supplementary information). At first, the HEK293 (β_3) cells appear on the surface with a rounded morphology and then, adopt an elongated spheroid shape with filipodal extensions. In contrast, the HEK293 (β_1) cells presented a limited spreading on the functionalized RGD surface (Figure 7-D). As QCM-D responses were very low for HEK293 (β_1), we assume that the observed cells on the diluted RGD surface are seeded cells.

Conclusions

The structural characterization of the SAMs carried out by using cyclic voltammetry and QCM-D reveal that single-component SAMs formed from pure EG_4OH, pure EG_6Biot and biotinylated mixed SAMs are packed without default. Biotin and hydroxyl-terminated thiols were assembled in a random distribution in the mixed SAMs without phase segregation. The SA surface density can be tuned by adjusting the percentage of EG_6Biot in the mixture of thiols used to prepare the SAMs. With this technique in hand, the density of adhesion ligand was easily controlled. We observed that surfaces displaying high density of RGD peptide are not specific whereas a critical interligand spacing of nearly 40 nm is mandatory to observe selective adhesion of $\alpha_v\beta_3$-expressing cells.

Today, numerous RGD-functionalized biomaterials, implants and nanoparticles for example, have the potential to revolutionize cancer diagnosis and therapy. Taken together, our findings offer a new paradigm to understand the *in vivo* behaviour of RGD-containing nanoparticles.[51] We are currently implementing this strategy for the design of a new generation of nanoparticles for drug delivery in cancer therapy.

Acknowledgements

This work was supported by the Nanoscience Foundation for scholarship of D. Thakar, and by the Agence Nationale de la Recherche, "Forcell" research support (ANR-12-BSV5-0021-01) and "Arcane" LabEx support (ANR-11-LABX-0003-01). We are grateful to NanoBio (Grenoble) for the facilities of the Synthesis Platform and of the Characterization of Interactions Platform.

Notes and references

Univ. Grenoble Alpes, DCM UMR 5250, F-38000 Grenoble, France; CNRS, DCM UMR 5250, F-38000 Grenoble, France

Electronic Supplementary Information (ESI) available: HPLC profiles and mass spectra of peptide compounds, additional data relative to structural characterization of the SAMs, SA adsorption and cell adhesion studies. See DOI: 10.1039/b000000x/

1 J. Robertus, W. R. Browne, B. L. Feringa, *Chem. Soc. Rev.,* 2010, **39**, 354–378.
2 M. D. Pierschbacher, E. Ruoslahti, *Nature,* 1984, **309**, 30-33.
3 U. Hersel, C. Dahmen, H. Kessler, *Biomaterials*, 2003, **24**, 4385-4415.
4 a) C. Roberts, C. S. Chen, M. Mrksich, V. Martichonok, D. E. Ingber, G. M. Whitesides, *J. Am. Chem. Soc.* 1998, **120**, 6548-6555. b) M. Mrksich, *Chem. Soc. Rev.*, 2000, **29**, 267-273.
5 M. Aumailley, M. Gurrath, G. Müller, J. Calvete, R. Timpl, H. Kessler, *FEBS Lett.,* 1991, **291**, 50-54.
6 M. Mammen, S. K. Choi, G. M. Whitesides, *Angew. Chem. Int. Ed.,* 1998, **37**, 2754-2794.
7 C. H. F. Wenk, F. Ponce, S. Guillermet, C. Tenaud, D. Boturyn, P. Dumy, D. Watrelot-Virieux, C. Carozzo, V. Josserand, J.-L. Coll. *Cancer Lett.,* 2013, **334**, 188-195.
8 (a) S. Foillard, Z. Jin, E. Garanger, D. Boturyn, M. Favrot, J.-L. Coll, P. Dumy. *ChemBioChem,* 2008, **9**, 2326-2332; (b) S. Foillard, L. Sancey, J.-L. Coll, D. Boturyn, P. Dumy. *Org. Biomol. Chem.,* 2009, **7**, 221-224.
9 (a) S. Foillard, P. Dumy, D. Boturyn. *Org. Biomol. Chem.,* 2009, **7**, 4159-4162 ; (b) L. Sandrin, L. Coche-Guerente, H. Basit, A. Bernstein, P. Labbé, P. Dumy, D. Boturyn. *Org. Biomol. Chem.,* 2010, **8**, 1531-1534.
10 K. Amschler, L. Erpenbeck, S. Kruss, M. P. Schön. *ACS Nano,* 2014, **8**, 9113–9125.
11 M. H. Lee, D. A. Brass, R. Morris, R. J. Composto, P. Ducheyne. *Biomaterials,* 2005, **26**, 1721-1730.
12 M. Rodahl, F. Höök, A. Krozer, P. Brzezinski, B. Kasemo, *Rev. Sci. Instrum.,* 1995, **66**, 3924-3930.
13 V. Heitmann, B. Reiß, J. Wegener, *Springer Ser. Chem. Sens. Biosens.,* 2007, **5**, 303-338.
14 M. Saitakis, E. Gizeli, *Cell. Mol. Life Sci.,* 2012, **69**, 357-371.
15 M. Tagaya, T. Ikoma, N. Hanagata, J. Tanaka, *Mater. Express,* 2012, **2**, 1-22
16 C. Fredriksson, S. Kihlman, M. Rodahl, B. Kasemo, *Langmuir,* 1998, **14**, 248-251.
17 N. Tymchenko, E. Nilebäck, M.V. Voinova, J. Gold, B. Kasemo, S. Svedhem, *Biointerphases* 2012, **7**:43, 1-9.
18 J. Fatisson, F. Azari, N. Tufenkji, *Biosens. Bioelectron.,* 2011, **26**, 3207-3212.
19 L. Nowacki, J. Follet, M. Vayssade, M. Vigneron, L. Rotellini, F. Cambay, C. Egles, C. Rossi, *Biosens. Bioelectron.,* 2015, **64**, 469-476.
20 a) M.S. Lord, C. Modin, M. Foss, M. Duch, A. Simmons, F.S. Pedersen, B.K. Milthorpe, F. Besenbacher, *Biomaterials,* 2006, **27**, 4529-4537. b) M.S. Lord, C. Modin, M. Foss, M. Duch, A. Simmons, F.S. Pedersen, F. Besenbacher, B.K. Milthorpe, *Biomaterials,* 2008, **29**, 2581-2587.
21 J. Li, C. Thielmann, U. Reuning, D. Johannsmann *Biosens. Bioelectron.* 2005, **20**, 1333-1340.
22 Z. Fohlerova, P. Skladal, J. Turanek, *Biosens. Bioelectron.,* 2007, **22**, 1896-1901.
23 G. Li, P. Yang, N. Huang, H. Ding, *J. Biosci. Bioeng.,* 2013, **116**, 235-245.
24 J. Kandel, H-S. Lee, P. Sobolewski, N. Tomczyk, R.J. Composto, D.M. Eckmann, *Biosens. Bioelectron.,* 2014, **58**, 249-257.
25 C. Satriano, G.M.L. Messina, C. Marino, I. Aiello, E. Conte, D. La Mendola, D.A. Distefano, F. D'Alessandro, G. Pappalardo, G. Impellizzerri, *J. Colloid Interf. Sci.,* 2010, **341**, 232-239.
26 D. Thakar, L. Coche-Guérente, M. Claron, C. H. F. Wenk, J. Dejeu, P. Dumy, P. Labbé , D. Boturyn, *ChemBioChem*, 2014, **15** (3), 377-381.
27 D. Boturyn, P. Dumy, *Tetrahedron Lett.,* 2001, **42**, 2787-2790.
28 a) D. Boturyn, J-L. Coll, E. Garanger, M. Favrot, P. Dumy, *J. Am. Chem. Soc.,* 2004, **126**, 5730-5739. b) E. Garanger, D. Boturyn, J-L. Coll, M. Favrot, P. Dumy, *Org. Biomol. Chem.,* 2006, **4**, 1958-1965.
29 K.L. Prime, G.M. Whitesides, *J. Am. Chem. Soc*., 1993, **115**, 10714-10721.
30 a) J. Spinke, M. Liley, F.-J. Schmitt, H.-J. Guder, W. J. Knoll, *Chem. Phys.,* 1999, **9**, 7012-7019. b) X. Su, Y-J. Wu, R. Robelek, W. Knoll, *Langmuir,* 2005, **21**, 348-353. c) O. Azzaroni, M. Mir, W. Knoll, *J. Phys. Chem., B* 2007, **111**, 13499-13503.
31 a) V.H. Perez-Luna, M.J. O'Brien, K.A. Opperman, P.D. Hampton, G.P. Lopez, L.A. Klumb, P.S. Stayton, *J. Am. Chem. Soc.,* 1999, **121**, 6469-6478. b) L.S. Jung, K.E. Nelson, P.S. Stayton, C.T. Campbell, *Langmuir,* 2000, **16**, 9421-9432. c) K.E. Nelson, L. Gamble, L.S. Jing, M.S. Boekl, E. Naeemi, S.L. Golledge, T. Sasaki, O.G. Castner, C.T. Campbell, P.S. Stayton, *Langmuir,* 2001, **17**, 2807-2816.
32 M. Riepl, K. Enander, B. Liedberg, *Langmuir,* 2002, **18**, 7016-7023.
33 M. Seifert, M.T. Rinke, H.J. Galla, *Langmuir,* 2010, **26** (9), 6386-6393.
34 G.V. Dubacheva, A. Van Der Heyden, P. Dumy, O. Kaftan, R. Auzély-Vélty, L. Coche-Guérente, P. Labbé *Langmuir,* 2010, **26**, 13976-13986.
35 S. Imabayashi, M. Iida, D. Hobra, Z.Q. Fong, K. Niki, T. Kakuichi, *J. Electroanal. Chem.,* 1997, **428** (1-2), 33-38.
36 J. Zheng, L. Li, S. Chen, S. Jiang, *Langmuir,* 2004, **20**, 8931- 8938.
37 G.K. Rowe, S.E. Creager, *Langmuir,* 1991, **7**, 2307-2312.
38. C.D. Bain, G.M. Whitesides, J. Am. Chem. Soc., 1989, 111, 7164-7175.
39 I. Reviakine, D. Johannsmann, R. P. Richter, *Anal. Chem.,* 2011, **83**, 8838-8848.
40 P. Bingen, G. Wang, N.F. Steinmetz, M.; Rodahl, R.P. Richter, *Anal. Chem.,* 2008, **80**, 8880-8890.
41 C. Fredriksson, S. Khilman, B. Kasemo, D.M. Steel, *J. Mater. Sc.: Mater. In Med.,* 1998, 9, 785-788.
42 M. Pfaaf, K. Tangemann, B. Müller, M. Gurrath, G. Müller, H. Kessler, R. Timpl, J. Engel, *J. Biol. Chem.,* 1994, **269**, 20233-20238.
43. E. Garanger, D. Boturyn, Z. Jin, P. Dumy, M.C. Favrot, J.L. Coll, *Molecular. Ther.,* 2005, **12**, 1168-1175.
44. As compounds **1** and **2** have an isoelectric point of 8, the net charge of the surface is positive at pH 7.4. See also: A. Ziegler, Adv Drug Deliv Rev., 2008, 60, 580-597.
45 M. Rodahl, F. Höök, C. Fredriksson, C.A. Keller, A. Krozer, P. Brzezinski, M. Voinova, B. Kasemo, *Faraday Discuss.,* 1997, **107**, 229-246.
46 V. Heitmann, B. Reiß, J. Wegener, *Springer Ser. Chem. Sens. Biosens.*, 2007, **5**, 303-338.
47 a) M. Arnold, E.A. Cavalcanti-Adam, R. Glass, J. Blümmel, W. Eck, M. Kantlehner, H. Kessler, J.P. Spatz, *ChemPhysChem,* 2004, **5**, 383-

388. b) E.A. Cavalcanti-Adam, A. Micoulet, J. Blümmel, J. Auernheimer, H. Kessler, J.P. Spatz, *Eur. J. Cell Biol.,* 2006, **85**, 219-224. c) E.A. Adam, T. Volberg, A. Micoulet, H. Kessler, B. Geiger, J.P. Spatz, *Biophys., J.* 2007, **92**, 2964-2974.

48 G.A. Hudalla, W.L. Murphy, *Langmuir*, 2009, **25**, 5737-5746.

49 S.P. Massia, J.A. Hubbell, *J. Cell Biol.*, 1991, 1089-1100.

50. L. Sancey, E. Garanger, S. Foillard, G. Schoehn, A. Hurbin, C. Albiges-Rizo, D. Boturyn, C. Souchier-Grichine, P. Dumy, J.-L. Coll, *Molecular Ther.,* 2009, **17**, 837-843

51. B. R. Smith, C. Zavaleta, J. Rosenberg, R Tong, J. Ramunas, Z. Liu, H. Dai, S. S. Gambhir, *Nano Today*, 2013, **8**, 126-137.

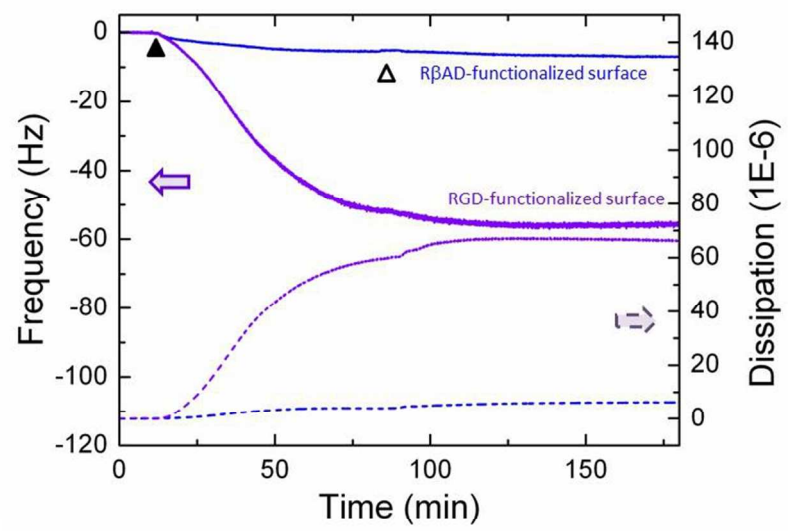

A critical interligand spacing is required to observe selective cell adhesion adhesion

254x190mm (96 x 96 DPI)